JOURNAL OF PROPULSION AND POWER
Vol. 13, No. 1, January–February 1997

Tip Clearance Flow–Shock Interaction in a Transonic Compressor Rotor

S. L. Puterbaugh*
U.S. Air Force Wright Laboratory, Wright–Patterson Air Force Base, Ohio 45433
and
M. Brendel†
University of Dayton, Dayton, Ohio 45409

A combination of experimental, computational, and analytical efforts were used to describe the phenomenological features of the interaction between the tip clearance flow and the passage shock in a transonic, axial compressor rotor. Unsteady static pressure was measured at the casing over the rotor, and steady measurements of total pressure and total temperature were made at the rotor exit. A fully three-dimensional, steady, Navier–Stokes computational fluid dynamics technique was used to obtain a solution to the flowfield at design conditions that compared favorably with the experimental measurements. Finally, a simple model was developed that predicts the kinematic and thermodynamic properties within the pre- and postshock vortex. Analysis of the numerical results revealed a wake-like nature of the vortex both upstream and downstream of the shock. The upstream character was strongly influenced by the injection of mass into the vortex via the clearance flow. The success of the simplified model's ability to predict the properties of the vortex within the interaction region allows two important conclusions to be drawn. First, the vortical character of the vortex upstream of the shock is not a significant factor in driving the interaction. Second, the interaction between the clearance flow and the shock is fundamentally the result of the change in momentum brought about by the shock-induced pressure rise. The interaction can therefore be viewed as an inviscid phenomenon.

Nomenclature

A = area
g_c = gravitational constant
h = enthalpy
$\dot{m}$ = mass flow
p = pressure
V = velocity

Subscripts
0 = total property
1 = cell inflow boundary
2 = cell outflow boundary
3 = flow injected into the cell
∞ = freestream

Introduction

METHODS of compressor design continue to lean heavily upon through-flow methods that employ models to describe various phenomena that are not captured by the simplified equations of motion. This remains true even with the continued development of computational fluid dynamics (CFD) methods because of the inability of CFD methods to be executed in design, or inverse, mode. Therefore, the development of models for through-flow methods continues to be an important part of compressor research efforts.

Efforts to generate advanced compressors necessarily extend outside design experience. Tools based on empiricism can be very misleading when used for advanced development. Therefore, it is important to develop physics-based models that can more confidently be used in this manner. This article describes the early efforts to develop such a model.

The largest potential for performance improvement lies in the tip region. The spanwise efficiency profile at the trailing edge of a typical transonic rotor reveals a fairly high, consistent efficiency from the hub to some point outboard of 50% span, where a severe reduction occurs. This is a result of the irreversibilities that occur in the tip region. In the case of transonic compressors, where overall adiabatic efficiency may exceed 90%, the efficiency in the tip region is generally well below 80%.

In the last 10 years, much effort has been spent on understanding and predicting the tip flow structure and loss in subsonic compressors.[1–3] However, the tip flowfield features that are peculiar to transonic compressors have only recently come under study. Four papers[4–7] have reported the presence of an interaction between the tip clearance vortex and the passage shock, which is a significant feature of the flowfield, along with a description of the phenomenon. The objective of the current work (based on Ref. 8) is twofold. First, the primary factors that drive the interaction between the clearance flow and the shock are examined. Secondly, a method is sought that can be used to model the interaction phenomenon for ultimate use in through-flow-type compressor design and analysis computer programs.

Background

Transonic compressor rotors are typically unshrouded, i.e., the rotor blade row rotates within a fixed duct with the tips of the blades set to some finite radial clearance. The magnitude of the clearance is determined by mechanical constraints and varies during operation as a function of rotational speed, thermal conditions, and transverse loads resulting from flight ma-

Presented as Paper 95-2459 at the AIAA/ASME/SAE/ASEE 31st Joint Propulsion Conference and Exhibit, San Diego, CA, July 10–12, 1995; received Aug. 14, 1995; revision received July 3, 1996; accepted for publication July 8, 1996.

*Aerospace Engineer, Aero Propulsion and Power Directorate, WL/POTF Building 18, 1950 Fifth Street.

†Assistant Professor, Mechanical and Aerospace Engineering Department, 300 College Park Avenue. Senior Member AIAA.

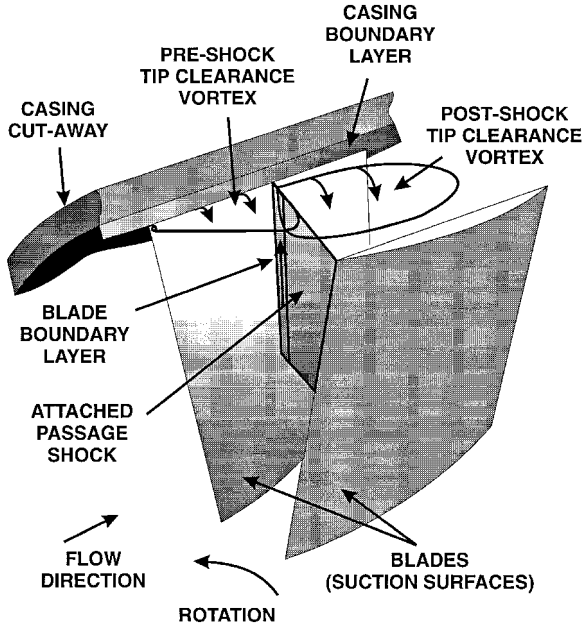

Fig. 1 Flow features in the tip region of the blade row.

neuvering. The flowfield that is induced by this geometry is extremely complex, being composed of both viscous and inviscid phenomena. The flow structures that are generally recognized as the significant factors include boundary layers on the blade surfaces and casing, tip clearance flow, secondary flow, and, for transonic rotors, shocks. Figure 1 illustrates these flow structures as they relate to a compressor rotor blade row. Each of these and, not incidentally, the interaction between them, plays an important role in determining the character of the tip flowfield.

A difference in pressure exists on either side of the blade because of the velocities induced on each surface. Just like the finite wing, these pressures tend to drive fluid around the blade tip from the pressure side to the suction side. In the case of the compressor, however, the fixed casing restricts and alters the flow. The fluid is driven through the tip clearance by the pressure difference and forms a jet that is subsequently directed by a combination of the effects of the through-flow and the casing boundary layer.[3,9] The resulting flow, termed tip clearance flow, dominates the tip flowfield.[10] It results in a loss in lift, i.e., less work in the outer span, an increase in blockage caused by the formation of a vortex on the suction side, and increased losses caused by the presence of shear layers between the vortex and the through-flow and interaction with the casing boundary layer.

The introduction of a shock into this already complex tip flowfield not only adds the entropy generation of the shock, but results in significant interactions with all of the flow structures mentioned previously. The interaction between the shock and the tip leakage vortex plays an important role in determining the nature of the tip flowfield. This has also been seen in other work.[4,5]

Approach

A combination of experimental and numerical modeling work was used to examine the interaction between the clearance flow and the shock. The experimental portion of the effort was performed during the swept rotor study (SRS) fan research program that was conducted at Wright Laboratory's Compressor Aero Research Lab. The numerical work was done using a steady-state fully three-dimensional Reynolds-averaged Navier–Stokes method.[11]

Rotor 4 of the program was the subject of the work described herein. Rotor 4 demonstrated state-of-the-art performance and has been the subject of several other studies.[5,7,12–14] The design point performance along with geometric parameters is shown in Table 1.

Instrumentation, Calibration, and Signal Processing

Measurements used to assess the tip flow structure included casing-mounted, unsteady static pressure and rotor-exit, steady-state total temperature, and pressure probe traverses.

A total of 10 high-frequency-response pressure transducers were mounted in the casing, as shown in Fig. 2, to make the unsteady static pressure measurements. The transducers were mounted in evenly spaced axial increments between 37.5% chord upstream of the rotor leading edge to 25% chord upstream of the rotor trailing edge. The screen on the transducer was positioned to within 0.010 in. of the flow path surface in the radial direction.

The transducers were calibrated before each test session by applying a known pressure to the transducer while installed in the test article and adjusting amplifier output to provide the required gain. The measured waveforms were used to supply the dynamic portion of the pressure signal, with the steady-state portion being supplied by a companion steady-state static-pressure tap.

A once-per-revolution synchronization pulse that provided rotor position information was recorded and digitized along with the transducer output. This was used to phase-lock the rotor such that subsequent ensemble-averaging and unsteadiness calculations would be done for the same blade passage on each revolution. The final representation of the signal from a given transducer was either in the form of an ensemble-averaged waveform or a waveform made up of rms values. A total of 125 sample functions was used to construct the ensemble-averaged and rms waveforms based on a study done by Sellin et al.[14]

A two-axis (radial and yaw) actuator was used to traverse the probes at the rotor exit. The resolution in the radial direction was 0.01 mm, with a repeatability of 0.025 mm and an overall accuracy in position of ± 0.05 mm. In the yaw direction, both the resolution and repeatability were 0.1 deg with an accuracy of ± 0.25 deg. Three probes were used to measure the rotor exit flowfield, a five-hole prism probe, a wedge probe, and a half-shielded thermocouple probe. The traverse probe data were acquired from 100 to 20% span at 2% increments. The steady-state traverse probes were calibrated in a freejet

Table 1 Design point performance and geometric parameters

Pressure ratio, 2.054
Adiabatic efficiency, 90.2%
Corrected specific flow, 42.95 lbm/s/ft^2
Corrected tip speed, 1500 ft/s
Inlet relative Mach number, 1.63
Mean rotor aspect ratio, 1.320
Rotor inlet hub/tip ratio, 0.312
Casing diameter, 17.0 in.
Mean tip clearance (% of chord), 0.6%

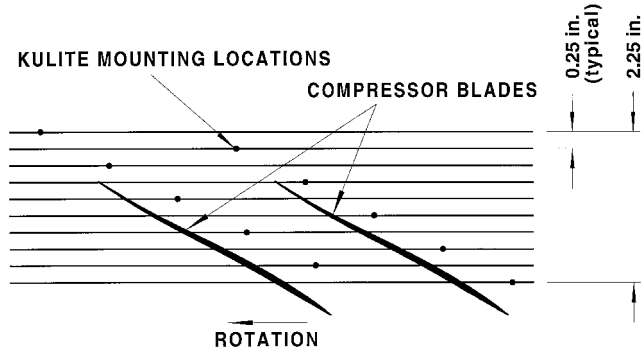

Fig. 2 Transducer mounting locations.

calibration facility. The calibration provided measurement corrections for both Mach number and pitch-angle variations.

Rotor to casing tip clearance was measured during test article operation by a discharge-type clearance measurement system.

Numerical Approach

The numerical method used for the current work was from Hah.[11] This approach utilized a fully three-dimensional, steady-state formulation of the Reynolds-averaged Navier–Stokes equations. The equations were solved using a finite volume approach, which produced a set of linear algebraic equations. The overall numerical scheme was second-order accurate in the physical domain.

The system of equations was closed using a k-ε type turbulence model to provide the Reynolds stresses. A low-Reynolds number correction was employed to extend the validity of the model to the viscous sublayer. This approach allowed the computational scheme to be utilized for flowfields containing strong secondary flows and flow separation. The constants in the turbulence transport equations were the same as those used in many earlier computations of the flowfield in transonic fans and compressors; they were not modified for the current work.

The upstream boundary conditions included specification of total pressure, total temperature, and flow angle. The downstream conditions included specification of static pressure at a point with asymptotic conditions enforced on other variables. Nonreflective boundary conditions are applied at the upstream and downstream boundaries. Periodicity is enforced at the circumferential boundaries. A no-slip condition is applied at all solid boundaries, including the blade and hub in the relative reference frame and the casing in the absolute frame.

For the current study, a total of 347,300 nodes made up the blade-centered I-type grid. Fifty nodes were used in the pitchwise direction, 46 nodes in the spanwise direction, and 151 nodes in the streamwise direction. The blade chord had 95 nodes distributed from leading edge to trailing edge. To resolve the clearance flow, seven nodes were distributed from suction surface to pressure surface with six nodes in the clearance gap.

Results and Discussion

The current study concentrated on the peak efficiency operating point at design speed. At this operating condition, the clearance was measured at 0.025 in. near the leading edge and 0.022 in. near the blade stack axis. This corresponded to 0.625 and 0.55% of chord, respectively.

Unfortunately, experimental methods that were capable of making direct kinematic and thermodynamic measurements of the phenomena under study were not available. Therefore, the experimental measurements were primarily used to support the CFD results. The first step was to validate the CFD results using the experimental measurements that were obtained.

Figure 3 shows a comparison between experimental measurement and the numerical solution of the spanwise total temperature distributions at the rotor exit. The uncertainty in temperature measurement was computed to be ±1.97°F at a 95% confidence interval. Total temperature from the numerical solution was circumferentially mass averaged to compare directly with the measurements. Both distributions reveal the significant increase in work near the casing, resulting from the severe diffusion in the relative frame caused by the interaction between the tip clearance flow and the shock, to be discussed later.

Spanwise distributions of total pressure are compared in Fig. 4. The agreement is not as good as in Fig. 3; however, the local increase in total pressure near the case (95% span) caused by the clearance flow is evident in both.

A detailed, quantitative comparison between spatially resolved, ensemble-averaged measured and computed tip static pressure was also done. Examples of comparisons at 12.5 and

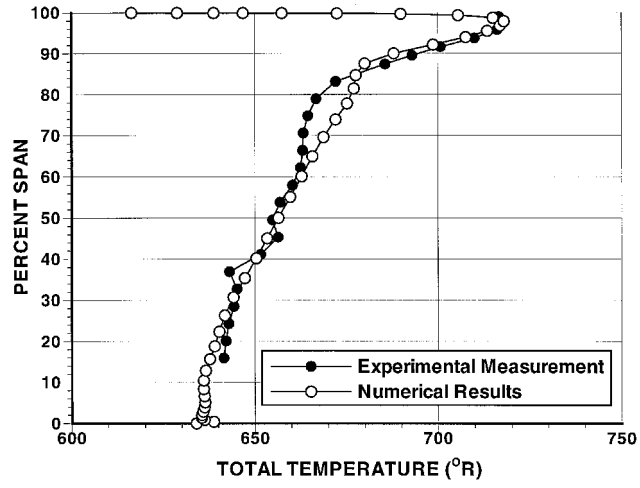

Fig. 3 Comparison between experimental measurements and the numerical solution spanwise total temperature distribution at the rotor exit.

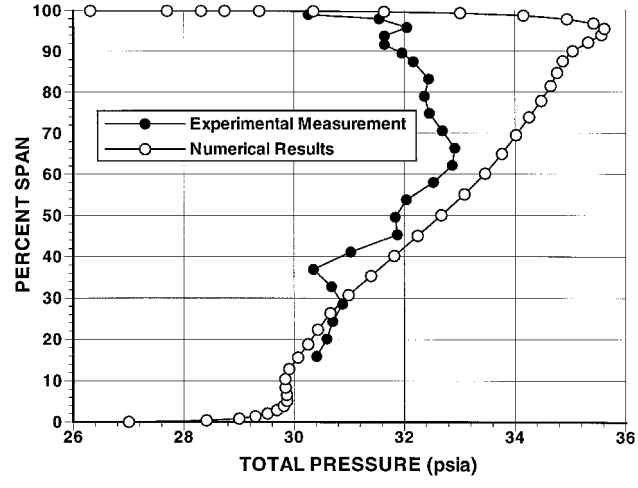

Fig. 4 Comparison between experimental measurements and the numerical solution spanwise total pressure distribution at the rotor exit.

37.5% chord are shown in Fig. 5. The steep rise in the positive x-axis direction corresponds to shocks, and the steep drop corresponds to the suction side of the blade. The uncertainty in pressure measurement using the casing-mounted high-frequency-response pressure transducers was computed to be ±0.086 psi at a 95% confidence interval.

Small differences are present because of the fact that the numerical solution was run at an operating point with a slightly higher back pressure than the measurement. This is indicated by a shift in shock position and a slightly higher average static pressure at 37.5% chord. In addition, higher gradients are seen in the numerical results than what was measured. This is, in general, because of the finite frequency response (nominally 100 kHz) of the recording/processing system vs the practically infinite frequency response of the numerical solution.

At each discrete time interval, which corresponds to pitchwise position of the static pressure signal, an unsteadiness parameter was computed. The unsteadiness parameter is defined as the rms variation of discrete readings divided by the local average. A contour plot of the data reveals the spatial orientation of unsteadiness within the blade passage at the tip. It should be emphasized that the data were processed such that the same passage was interrogated in successive revolutions. Therefore, the unsteadiness contains no effect of blade-to-blade variation, but only the unsteadiness generated within a given passage because of locally unsteady phenomena.

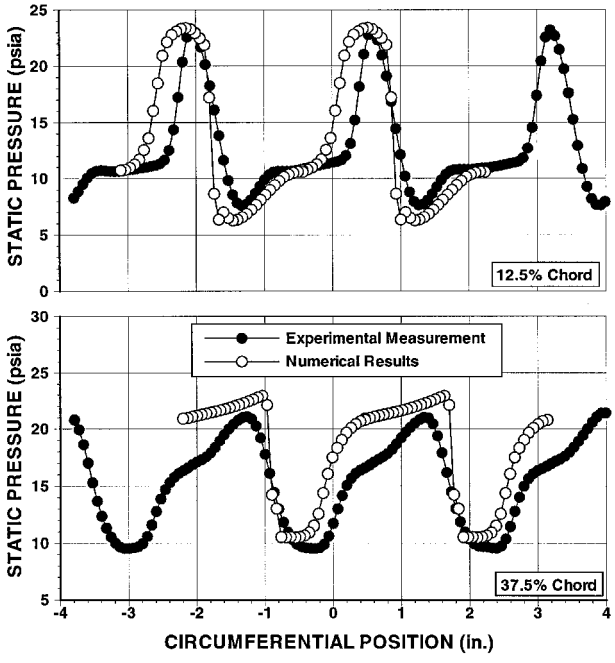

Fig. 5 Comparison between measured and predicted static pressure at 12.5 and 37.5% chord.

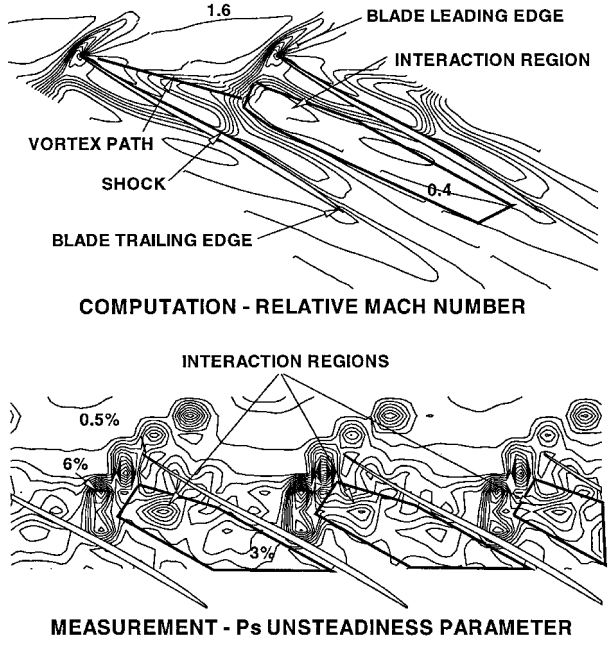

Fig. 6 Measured static pressure unsteadiness parameter and computed Mach number distributions at 97.5% span at the peak efficiency operating point.

Figure 6 compares the unsteadiness parameter to Mach number contours obtained from the numerical solution at 97.5% span at the peak efficiency, design speed operating point. A detailed discussion of the unsteadiness and its significance was given by Puterbaugh and Copenhaver.[7] We will concentrate here on the peak in unsteadiness that occurs at midpitch.

A local peak of unsteadiness occurs just downstream of the shock near midpitch and extends downstream, moving toward the pressure surface with increasing downstream distance. The location of this unsteadiness near the shock implies that the shock plays a part in its generation or, at the least, is influenced by its action. The fact that the tip leakage vortex impacts the passage shock at about this location has been established by several researchers through both experimental and numerical studies.[4–6,15] Furthermore, in fundamental studies of shock–vortex interaction, the interaction has been shown to be unsteady for both strong and weak interactions.[16,17] Therefore, it is proposed that the unsteadiness indicates the presence of a coherent structure that results from the interaction between the clearance flow and the passage shock.

The Mach number contours reveal an extremely low Mach number region in precisely the same location as the midpitch unsteadiness. The flow expands around the leading edge to a Mach number of a little over 1.6, and then encounters a slight precompression region upstream of the shock. The shock position is indicated by the tight grouping of contour lines that extends from just upstream of the leading edge to the suction surface approximately normal to the streamwise direction. The sonic line bulges at the point of vortex impact against the shock. Just downstream of the bulge, the Mach number falls rapidly to a value slightly below 0.4. To generate a Mach number this low downstream of a normal shock, the upstream Mach number would have to be about 6.5. However, the upstream Mach number peaks just above 1.6.

The spatial similarity of the midpassage unsteadiness peak and the low Mach number region implies that they represent the same structure. The source of the unsteadiness could be because of the unsteady shock position and its nonlinear effect on the entrance flow. As a minimum, unsteadiness would be expected to exist at the high-/low-velocity interface between the flow in the interaction region and the freestream.

To further clarify the link between the measured and computed results, a comparison similar to that in Fig. 6 was made at the near-stall operating point, and this is shown in Fig. 7. Both plots show that the interaction region remains in about the same location and retains about the same shape as it did at peak efficiency. In the experimental results contour plot, the magnitude of the unsteadiness parameter in this region increased from about 2.5% at peak efficiency to about 4.3% at near stall. Whereas, in the numerical results, the Mach number in the interaction region reduced from about 0.4 at peak efficiency to about 0.2 at near stall. Clearly, both cases show that the interaction region responds to increasing back pressure by increasing the intensity of the phenomenon relative to the remainder of the flowfield.

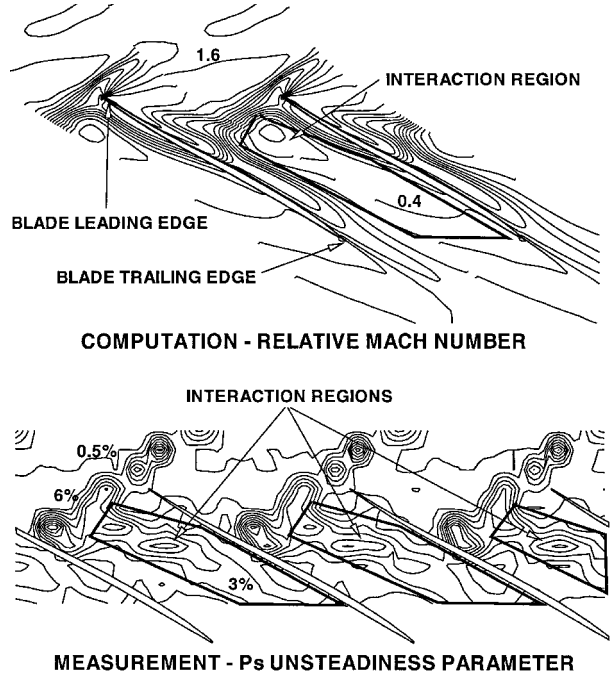

Fig. 7 Measured static pressure unsteadiness parameter and computed Mach number distributions at 97.5% span at the near-stall operating point.

Clearance Flow-Shock Interaction

Figure 8 shows traces of the paths of particles that were released within the clearance gap, at about midgap, over the rotor tip. The traces generated from the leading edge to about 50% chord emerge from the gap in a direction almost normal to the chord. The particles released from the trailing-edge half of the blade turn more quickly into the streamwise direction. The change in shape of the paths is caused by the change in pressure difference across the blade, as shown in Fig. 9. The pressure difference across the blade reduces sharply at the chordwise location where the passage shock intersects the suction surface. Many researchers have shown that the clearance flow is pressure driven; therefore, where the pressure difference is greatest, the clearance flow occurs at a higher speed in a jet-like fashion. The momentum induced on the clearance flow in the upstream portion of the chord then carries the flow out into the passage as shown. In the downstream section, the clearance flow is accelerated to a lower speed and, therefore, the streamwise momentum imposed by the passage flow is better able to turn the clearance flow in the streamwise direction.

A vortical pattern is clearly shown in Fig. 8 by the roll-up of particle traces beginning at the leading edge and extending out into the passage. The vortex continually entrains fluid that emerges from the clearance gap up to the point of intersection of the passage shock and the suction surface. Downstream of the shock/suction surface intersection point, the clearance flow is no longer entrained into the vortex.

Contours of static pressure are shown in Fig. 9. The contours are drawn in increments of 2.0 psi. Again, the vortex path is indicated on the plot. Pressure increases, in general, from upstream to downstream under the diffusing action of the passage. A global minimum of pressure occurs near the leading edge within the vortex. The pressure then increases slightly inside the vortex until the vortex impacts the shock. The shock is indicated by the grouping of contour lines lying approximately normal to the streamwise direction. Note that unlike the Mach number contours, there is no strong effect on pressure where the vortex impacts the shock. In fact, downstream of the shock, the pressure is fairly constant normal to the streamwise direction.

The velocity distribution is not shown here, but is similar in structure to the Mach number contours. A defect in velocity exists at the core of the vortex upstream of the shock. This is a direct result of the injection of the low-streamwise-momentum clearance flow into the vortex. The velocity defect at midpitch, in combination with the fact that the static pressure is fairly constant normal to the streamwise direction, implies that this flow structure is wake-like in nature.

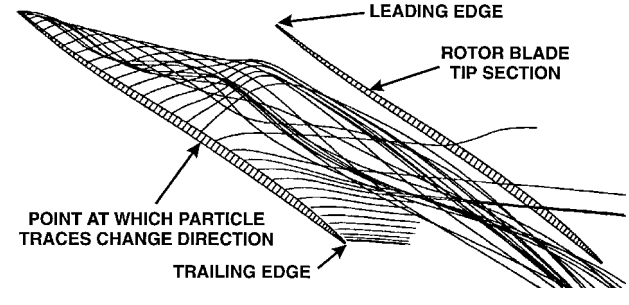

Fig. 8 Particle traces generated by releasing particles from within the tip gap determined from the numerical solution.

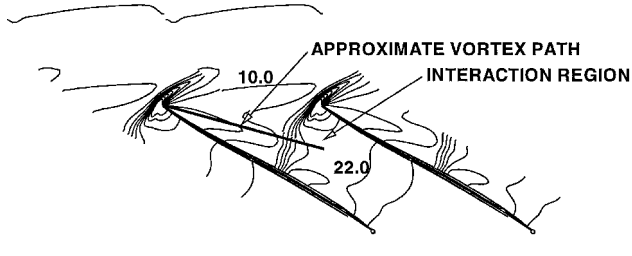

Fig. 9 Static pressure contours from the numerical solution at 97.5% span.

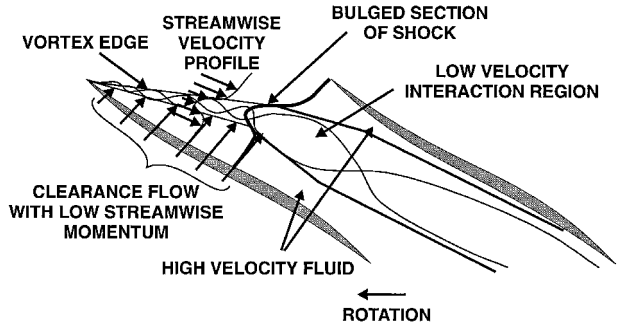

Fig. 10 Schematic diagram of clearance flow–shock interaction in a compressor cascade.

Communication between the vortex and core flow is through pressure. Therefore, when the freestream undergoes an abrupt change in conditions across the shock, both the freestream and the low-velocity flow within the control volume react accordingly. The freestream, which encounters the shock at a fairly high Mach number, undergoes the change in properties according to the well-known shock relations. The clearance flow, on the other hand, approaches the shock at a fairly low, yet still supersonic, Mach number. The downstream back pressure is elevated by the shock in the freestream, which causes a significant reduction in the velocity of the clearance flow by reducing the streamwise momentum. Therefore, the Mach number in the downstream clearance flow is far below what is expected, simply by the action of a shock.

Figure 10 shows a schematic diagram of the processes that occur in clearance flow–shock interaction, which were just discussed. The view is over the rotor blade tips. Storer and Cumpsty[2] and Crook et al.,[18] among others, state that the tip clearance vortex dominates the endwall flowfield in a subsonic axial compressor. Based on Figs. 6–9, it is clear that the interaction between the tip clearance vortex and the passage shock dominates the endwall flowfield in a transonic or supersonic compressor.

Clearance Flow–Shock Interaction Model

The foregoing discussions suggest that the clearance flow–shock interaction be proposed as primarily dependent upon mass injection and a wake-like vortex core both upstream and downstream of the shock. These two attributes are not independent since the mass injection assures a wake-like vortex core upstream of the shock. The presence of a wake-like downstream structure allows the static pressure rise that is generated by the shock to influence the behavior of the vortex as it traverses the shock.

Furthermore, it is proposed that the vortical nature of the structure is not a significant factor in the clearance flow-shock interaction process, but that the structure is dominated by the wake-like nature. This assumption allows the flow properties within the vortex and interaction region to be governed only by the streamwise component of the momentum equation.

The proposed model of the vortex and its interaction with the shock is shown schematically in Fig. 11. An axisymmetric control volume is assumed to enclose the vortex, separating the vortex fluid from the freestream. The core flow is not allowed to cross the control surface except at the upstream boundary. Only the mass that constitutes the clearance flow is allowed to cross the control surface being injected as a function of streamwise distance. The shape of the control volume results from the mass injection and pressure forces and is a part of the solution. Storer and Cumpsty[9] suggested computing

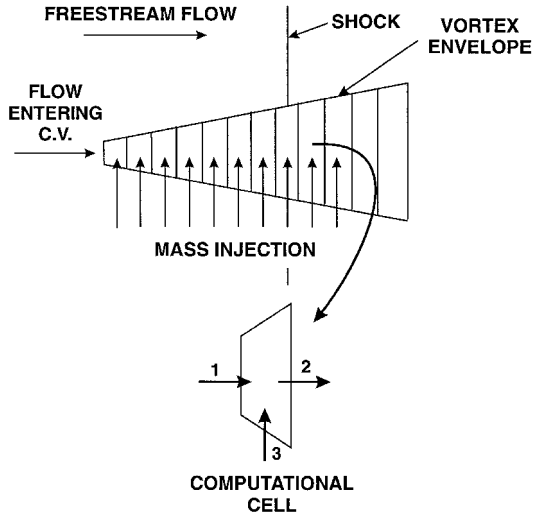

Fig. 11 Schematic diagram of the clearance flow–shock interaction model.

the loss generated by the clearance flow using a similar modeling approach.

Quasi-one-dimensional flow was assumed to exist inside the control volume, with the only external influence being pressure forces from the freestream and the injected mass flow. The axial extent of the domain of interest was subdivided into an arbitrary number of equal-length segments, or cells. The shock was arbitrarily positioned to the middle of one of the cells. The model was kept simple by using a noniterative, marching procedure. Therefore, it was assumed that the injected mass flow and the incoming flow from the upstream cell boundary was fully mixed at the downstream cell boundary. Downstream static pressure is assumed equal to the freestream value at that cell face to close the system of equations.

The assumptions just discussed, when applied to the conservation equations, give the following governing equation set:

$$\dot{m}_1 + \dot{m}_3 = \dot{m}_2 \tag{1}$$

$$\dot{m}_1 V_1 - \dot{m}_2 V_2 + g_c[p_1 A_1 + p_\infty (A_2 - A_1) - p_2 A_2] = 0 \tag{2}$$

$$\dot{m}_1 h_{0_1} + \dot{m}_3 h_{0_3} = \dot{m}_2 h_{0_2} \tag{3}$$

Velocity is the unknown at the downstream boundary of each cell. When the cell is upstream or downstream of the shock, the pressure forces balance and the momentum equation reduces to a rearrangement of Eq. (2). At the cell that contains the shock, the pressure jump caused by the shock must be considered. The pressure at the upstream cell boundary is set equal to the upstream, freestream value. The normal shock relation for static pressure at the shock Mach number is used to obtain the pressure at the downstream cell boundary. The pressure at the cell wall is set equal to the average of the upstream and downstream pressures. The pressure forces no longer balance and a quadratic equation in V_2 results.

Four different conditions must be specified to the model. First, the cell farthest upstream, where the computation will begin, must admit a specified amount of freestream fluid into the control volume. The initial momentum is set by the flow crossing the upstream boundary and strongly influences the velocity distribution in the remainder of the domain. Second, the mass injection must be specified for each cell. This mass injection function models the effect of the clearance flow as it is entrained into the vortex. Third, the upstream, freestream conditions must be specified, which include Mach number, total pressure, and total temperature. Finally, a shock Mach number must be specified independently to accommodate the nonideal nature of the shock pressure rise.

The model was executed for the peak efficiency operating point discussed earlier. The mass injection function (Fig. 12) used in the model was determined from the numerical solution. Various properties obtained from the numerical solution along the vortex path are compared with the model results. The thorough evaluation of the computational results allows the computational results to be used as the standard by which the model's results will be judged.

Figure 13 shows a comparison of the axial distribution of vortex radius between the numerical results and the model results. The radii from the numerical results were determined from the edge of the cone created by the particle traces in Fig. 8. The vortex computed in the numerical solution was oval in cross section rather than circular. Therefore, this comparison only takes the vortex structure in the cascade plane into account. The spanwise extent of the structure was no more than 5% immersion from the case, with an influence on flow parameters to about 20% immersion.

The model gives the streamwise area distribution of the vortex; the radius distribution is computed assuming that the area is circular in shape. The overall vortex size resulting from the model agrees fairly well with the numerical results; however, the rate of increase of radius with downstream distance differs. The model generates a large vortex radius at the leading edge that is clearly inappropriate. This results from the requirement to admit a sufficient quantity of freestream flow to restrict the Mach number entering the cell containing the shock to about sonic.

Note that the shock is indicated at 50% chord here (vs 60% in Fig. 12). This is because of the difference in the chordwise

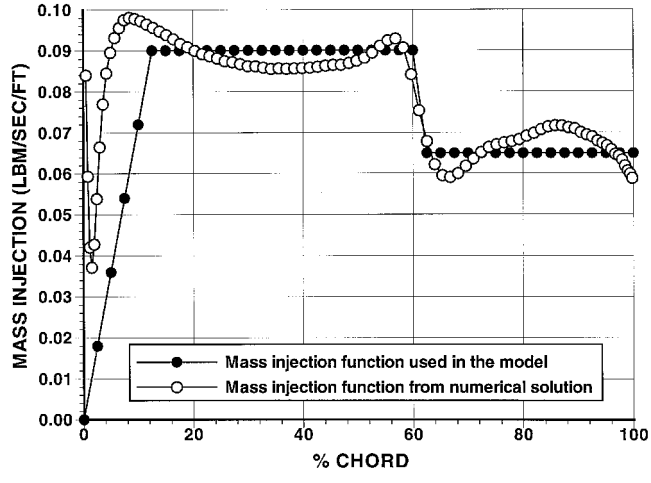

Fig. 12 Mass flow injection function used in the model.

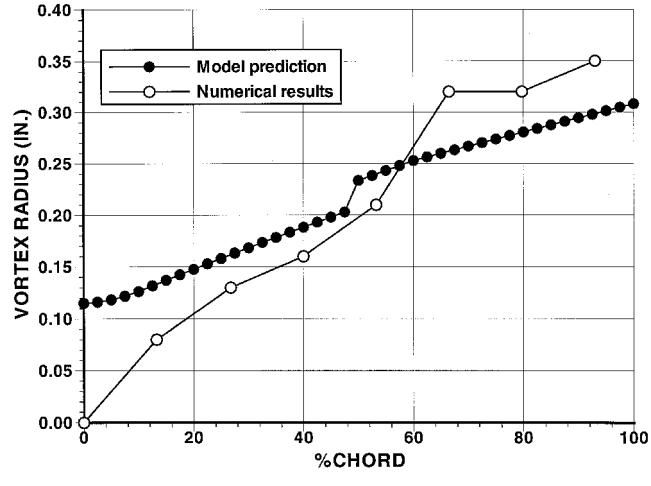

Fig. 13 Vortex radius as a function of axial distance.

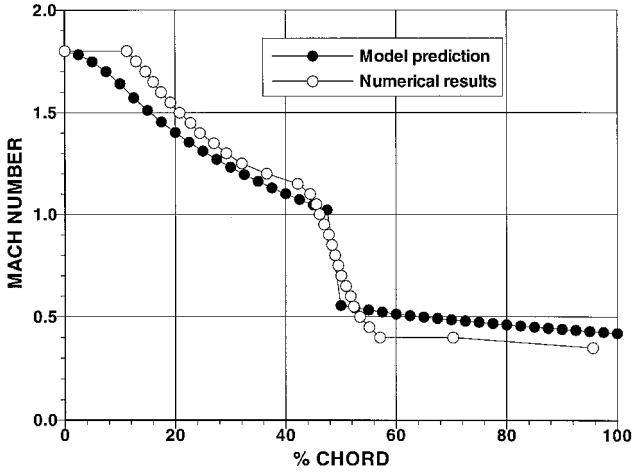

Fig. 14 Axial Mach number comparison between the model and numerical results.

location of the vortex/shock intersection (Figs. 13 and 14) and the suction surface/shock intersection (Fig. 12).

Figure 14 shows the streamwise distribution of axial Mach number determined from the model as compared to the numerical results. The two curves agree quite well in terms of overall shape and level. The effect of the shock is clearly seen at about midchord where the Mach number drops from just over sonic upstream to about 0.5 downstream.

The severe diffusion of the clearance flow, which is the essence of the interaction between the clearance flow and the shock, is successfully predicted by the model. Therefore, since the model is based only on the change in pressure at the shock and its influence on streamwise momentum, it follows that this is most important in the physics of the interaction process.

The interaction model is intended to eventually be incorporated into an axisymmetric through-flow compressor design and analysis computer program. The model would be used to predict the blockage increase in the tip region caused by clearance flow–shock interaction. It is envisioned that additional models would be available to predict shock position and clearance flow rate that are critical to the accuracy of the clearance flow–shock interaction model.

Conclusions

A description of the physics that drive the tip clearance flow–shock interaction process is developed in the work presented here. The interaction between the clearance flow and the shock has only recently come under study. Adamczyk et al.,[4] Copenhaver et al.,[5] and Suder and Celestina[6] have each described the interaction in varying degrees of completeness. The current work has built upon the observations of these papers and provided a framework for increased understanding of the complex tip region flowfield of a transonic compressor rotor. The significant findings are as follows:

1) The postshock vortex has a wake-like nature. This characteristic allows the transmission of the freestream pressure to the core of the postshock vortex to decelerate the vortex, or clearance flow, in an abrupt manner in response to the shock-induced pressure rise in the freestream.

2) The injection of mass via the clearance flow plays an important role in the clearance flow–shock interaction process. The mass injection governs the wake-like nature of the vortex upstream of the shock. The low-velocity core of the upstream vortex has a significant impact on the overall interaction.

3) The vortical character of the vortex upstream of the shock is not a significant factor in driving the interaction. The model essentially assumed that the vortex was a wake, with zero tangential velocity, yet the streamwise distribution of properties associated with the interaction was predicted quite well.

4) The interaction between the clearance flow and the shock is fundamentally the result of the change in momentum brought about by the shock-induced pressure rise. The interaction can therefore be viewed as an inviscid phenomenon. Understanding what drives the interaction is the first step in determining overall design strategies or novel approaches that can reduce the negative effect of the interaction on rotor performance.

Acknowledgments

The authors acknowledge the work done by General Electric Aircraft Engines for the design of the subject rotor under U.S. Air Force Contract F33615-80-C-2059. The authors also thank the U.S. Air Force for the opportunity to pursue this research and publish the results, and they acknowledge the research staff at the Compressor Aero Research Lab for their work on the project. Special thanks go to Chunill Hah for his work in obtaining the numerical solutions that were vital to this work.

References

[1]Chen, G. T., Greitzer, E. M., Tan, C. S., and Marble, F. E., "Similarity Analysis of Compressor Tip Clearance Flow Structure," *Journal of Turbomachinery*, Vol. 113, No. 2, 1991, pp. 260–271.

[2]Storer, J. A., and Cumpsty, N. A., "Tip Leakage Flow in Axial Compressors," *Journal of Turbomachinery*, Vol. 113, No. 2, 1991, pp. 252–259.

[3]Inoue, M., and Kuroumaru, M., "Structure of Tip Clearance Flow in an Isolated Axial Compressor Rotor," *Journal of Turbomachinery*, Vol. 111, No. 3, 1989, pp. 250–256.

[4]Adamczyk, J. J., Celestina, M. L., and Greitzer, E. M., "The Role of Tip Clearance in High-Speed Fan Stall," *Journal of Turbomachinery*, Vol. 115, No. 1, 1993, pp. 28–39.

[5]Copenhaver, W. W., Hah, C., and Puterbaugh, S. L., "Three-Dimensional Flow Phenomena in a Transonic, High-Through-Flow, Axial-Flow Compressor Stage," *Journal of Turbomachinery*, Vol. 115, No. 2, 1993, pp. 240–248.

[6]Suder, K. L., and Celestina, M. L., "Experimental and Computational Investigation of the Tip Clearance Flow in a Transonic Axial Compressor Rotor," *Journal of Turbomachinery*, Vol. 118, No. 2, 1996, pp. 218–229.

[7]Puterbaugh, S. L., and Copenhaver, W. W., "Flowfield Unsteadiness in the Tip Region of a Transonic Compressor Rotor," *Proceedings of Unsteady Flows in Aeropropulsion*, American Society of Mechanical Engineers, New York, 1994, pp. 77–86.

[8]Puterbaugh, S. L., "Tip Clearance Flow-Shock Interaction in an Advanced, Transonic, Axial-Flow Compressor Rotor," Ph.D. Dissertation, Univ. of Dayton, Dayton, OH, Dec. 1994.

[9]Storer, J. A., and Cumpsty, N. A., "An Approximate Analysis and Prediction Method for Tip Clearance Loss in Axial Compressors," *Journal of Turbomachinery*, Vol. 116, No. 4, 1994, pp. 648–656.

[10]Cumpsty, N. A., *Compressor Aerodynamics*, Longman Scientific and Technical, Essex, England, UK, 1989.

[11]Hah, C., "Calculation of Three-Dimensional Viscous Flows in Turbomachinery with an Implicit Relaxation Method," *Journal of Propulsion and Power*, Vol. 3, No. 5, 1987, pp. 415–422.

[12]Hah, C., and Puterbaugh, S. L., "A Critical Evaluation of a Three-Dimensional Navier-Stokes Method as a Tool to Calculate Transonic Flows Inside a Low-Aspect-Ratio Compressor," CP-510, AGARD, Feb. 1992.

[13]Hah, C., Puterbaugh, S. L., and Copenhaver, W. W., "Unsteady Aerodynamic Flow Phenomena in a Transonic Compressor Stage," AIAA Paper 93-1868, June 1993.

[14]Sellin, M. D., Puterbaugh, S. L., and Copenhaver, W. W., "Tip Shock Structures in Transonic Compressor Rotors," AIAA Paper 93-1869, June 1993.

[15]Freeman, C., "Effect of Tip Clearance on Compressor Stability and Engine Performance," *Tip Clearance Effects in Axial Turbomachinery*, von Kármán Inst. Lecture Series 1985-05, Rhode-Saint-Genese, Belgium, 1985.

[16]Metwally, O., Settles, G., and Horstman, C., "An Experimental Study of Shock Wave/Vortex Interaction," AIAA Paper 89-0082, Jan. 1989.

[17]Cattafesta, L. N., III, and Settles, G. S., "Experiments on Shock/Vortex Interaction," AIAA Paper 92-0315, Jan. 1992.

[18]Crook, A. J., Greitzer, E. M., Tan, C. S., and Adamczyk, J. J., "Numerical Simulation of Compressor Endwall and Casing Treatment Flow Phenomena," *Journal of Turbomachinery*, Vol. 115, No. 3, 1993, pp. 501–512.